Climate
of the Past
Discussions

1 **Early Twentieth Century Southern Hemisphere Cooling**

2 Stefan Brönnimann,[1,2] Yuri Brugnara,[1,2,*] Clive Wilkinson[3]

3 *[1]Institute of Geography, University of Bern, Switzerland*

4 *[2]Oeschger Centre for Climate Change Research, University of Bern, Switzerland*

5 *[3]CSW Associates and Climatic Research Unit, University of East Anglia, Norwich, UK*

6 *[*] now at Empa, Laboratory for Air Pollution and Environmental Technology, Dübendorf, Switzerland*

7

8 *Corresponding author: S. Brönnimann, stefan.broennimann@unibe.ch*

9

10 **Abstract**

11 Global surface air temperature increased by ca. 0.5 °C from the 1900s to the mid-1940s, also known as Early

12 Twentieth Century Warming (ETCW). However, the ETCW started from a particularly cold phase, peaking in

13 1908-1911. The cold phase was global but more pronounced in the Southern Hemisphere than in the Northern

14 Hemisphere and most pronounced in the Southern Ocean, raising the question whether uncertainties in the data

15 might play a role. Here we analyse this period based on reanalysis data and reconstructions, complemented with

16 newly digitized ship data from 1903-1916 as well as land observations. The cooling is seen consistently in

17 different data sets, though with some differences. Results suggest that the cooling was related to a La Niña-like

18 pattern in the Pacific, a cold tropical and subtropical South Atlantic, a cold extratropical South Pacific, and cool

19 Southern midlatitude land areas. The Southern Annular Mode was positive, with a strengthened Amundsen-

20 Bellingshausen seas low, although the spread of the data products is considerable. All results point to a real

21 climatic phenomenon as the cause of this anomaly and not a data artefact. Atmospheric model simulations are

22 able to reproduce temperature and pressure patterns, consistent with a real and perhaps ocean-forced signal.

23 Together with two volcanic eruptions just before and after the 1908-1911 period, the early 1900s provided a

24 cold start into the ETCW.

25

26 **1   Introduction**

27 Global warming since the early 20th century proceeded in two phases, the so-called Early Twentieth

28 Century Warming (ETCW) from ca. 1905 to 1945 (Brönnimann, 2009, see review by Hegerl et al.,

29 2018) followed by a plateau phase in the 1950s and 1960s, and the strong warming since 1970. The

30 ETCW has been a matter of keen scientific interest, but the focus was mostly on the trend or on the

31 peak phase in the 1940s. Interestingly, the ETCW started with a clear dip in global temperatures

32 around 1910, which is more pronounced in sea-surface temperature (SST) than over land and which,

33 if analysed spatially, is most pronounced in the Southern Hemisphere (Hegerl et al., 2018). If real, one

34 might expect to find anomalous atmospheric circulation along with this change.

35   Atmospheric circulation during the first decade of the 20th century has not received much attention,

36   particularly not in the Southern Hemisphere. The Southern Oscillation Index (SOI) shows a tendency

37   towards a strengthened Walker circulation (Cane, 2005). Reconstructions of the Southern Annular

38   Mode (SAM) (e.g., Abram et al., 2014) indicate neutral values. The most comprehensive analysis was

39   performed by Connolly (2020) and Fogt and Connolly (2021). They presented a new reconstruction of

40   pressure back to 1905 and found that the SAM signal also dominated in the early 20th century,

41   however, without addressing specifically this period. They also found considerable differences

42   between station-based data sets and reanalyses. Northward of 60° S, the "Twentieth Century

43   Reanalysis" for this period (20CRv3, Slivinski et al., 2019) fits best with their reconstruction whereas

44   other products showed spurious trends. Poleward of 60° S the quality of all products deteriorates prior

45   to 1957 due to the sparseness of pressure data. There is thus a need to improve reconstructions of

46   Southern Hemisphere atmospheric circulation in the early 20th century.

47   Based on the assessment by Fogt and Connolly (2021), 20CRv3 is a good starting point for studying

48   this period. However, although it is widely and successfully used, very little pressure data was

49   ingested into 20CRv3 during these years. In fact, the ICOADS archive (Freeman et al., 2017) shows

50   massive gaps in the South Atlantic for this period. In this paper, we present newly digitised ship log

51   data and incorporate them into 20CRv3 in an offline assimilation approach (following Brönnimann,

52   2022). In addition to pressure from ships, we also assimilated one pressure series and five temperature

53   series from land stations. A second data set on atmospheric circulation used in this study is the

54   palaeoreanalysis ModE-RA (Valler et al., 2023ab), which combines model simulations and monthly-

55   to-seasonal observations in an offline approach. Results based on these data sets are compared with

56   purely observation-based data sets.

57   The paper is organised as follows. Section 2 presents the digitised ship logs and the data assimilation

58   approach. In Section 3 we show the results from all data products. These are discussed in light of

59   previous literature on the subject in Section 4. Conclusions are drawn in Section 5.

60

61   **2   Data and method**

62   **2.1   Digitising of log books**

63   We digitised the logs from 13 ships during the period 30 Apr. 1902 to 20 Sep. 1916 (Table 1). The

64   ships were selected such as to give a good coverage of the Southern Ocean during the period of study.

65   The tracks of the ships are shown in Fig. 1. Note that only one ship used the Panama canal, opened in

66   1914, giving a comparably good coverage of the Southern Ocean. In total we digitised 434'000

67   observations made at 64'080 observation times. All data were submitted to ICOADS.

68   For the application in this paper, we only used data in the Southern Hemisphere. Furthermore, of the

69   4-hourly pressure data we used only those within +/-2 hours of 12 UTC. Note that only pressure was

70   later assimilated; for temperature, a correction of the diurnal cycle would have been necessary, for

71   which we have too little information. Also, SST data from many of the ships were already in the

72   boundary conditions of 20CRv3.

73   This filtering restricts the number of observations. For the assimilation, we use 8063 measurements

74   made on 4209 days (1.92 measurement per day). The data cover the period 11 May 1902 to 25 Aug

75   1916. They are seasonally well distributed. In terms of the latitudinal distribution, 75% of the data are

76   between 30° and 60° S, 42% between 40° and 50° S.

77
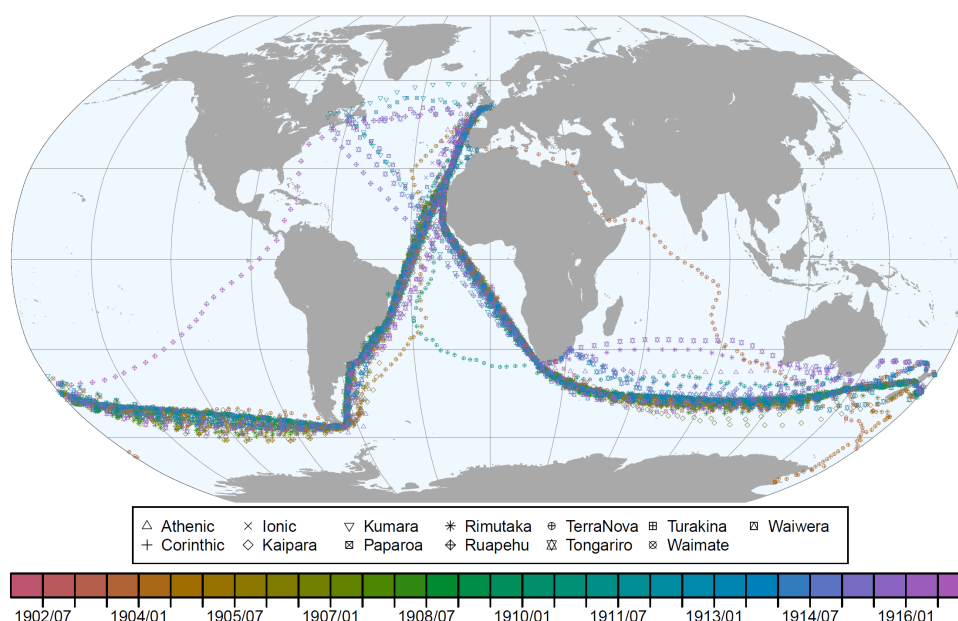
Fig. 1. Map of the tracks of the 13 ships for which data were digitised, coloured by year. Coordinates are shown

79   for 12 UTC, when they were measured.

80   **Table 1.** Periods covered by the ship logs, number of 12 UTC measurements assimilated, correlation with

81   20CRv3 and with 20CRv3+.

Ship	period	n	r_{20CRv3}	$r_{20CRv3+}$
Athenic	1905-1916	1208	0.78	0.98
Corinthic	1904-1907	312	0.84	0.86
Ionic	1904-1914	1349	0.81	0.96
Kaipara	1904-1908	157	0.87	0.97
Kumara	1911-1913	251	0.81	0.99
Paparoa	1905-1906	200	0.77	0.73
Rimutaka	1905-1916	1064	0.80	0.97
Ruapehu	1904-1916	316	0.71	0.94
Terra Nova	1903-1913	257	0.94	0.99
Tongario	1904-1916	1450	0.76	0.93
Turakina	1904-1915	431	0.81	0.99
Waimate	1902-1912	221	0.83	0.98
Waiwera	1913-1916	352	0.86	0.99

82

3

Climate
of the Past
Discussions

83   In addition, we also assimilated daily (12 UTC) series from land stations. This concerns one pressure

84   series that was not assimilated in 20CRv3 (Cape Town) as well as 5 temperature series from Uruguay,

85   South Africa, and Australia (see Table 2). The measurement hours did not change, hence, no further

86   adjustment of the diurnal cycle was necessary and the adjustment of the observations to 20CRv3, as is

87   described in the following, is sufficient. Note that further data would be available (e.g., pressure from

88   Buenos Aires), but is not yet digitised. The number of assimilated observations per year is shown in

89   Fig. 2.

90   **Table 2.** Land stations assimilated, latitude and longitude of the stations, variable (T = temperature, p =

91   pressure), number of 12 UTC measurements assimilated, correlation with 20CRv3 and with 20CRv3+ (note that

92   temperature data were deseasonalized).

Station	Lat	Lon	var.	n	r_{20CRv3}	$r_{20CRv3+}$
Melbourne	-37.81	144.97	T	10955	0.76	0.96
Kent Town	-34.92	138.62	T	10919	0.43	0.51
Sydney	-33.86	151.21	T	10955	0.67	0.86
Rocha	-34.49	-54.31	T	9002	0.63	0.78
Cape Town	-33.93	18.48	T	10224	0.59	0.89
Cape Town	-33.93	18.48	p	10924	0.83	0.96

93
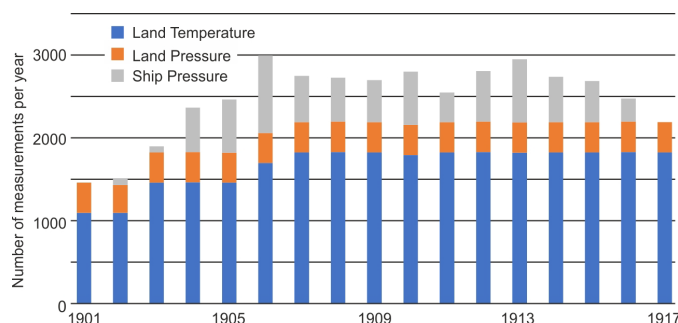
94

95   **Fig. 2.** Number of measurements per year in the period 1901-1917 (the numbers remain constant up to 1930 as

96   no further ship data were digitised and no land data are missing).

97

98   **2.2   The Twentieth Century Reanalysis**

99   The Twentieth Century Reanalysis (20CR) is a global dynamical reanalysis that is based on

100   assimilating surface pressure and sea-level pressure (SLP) data into an ensemble of atmospheric

101   model simulations (Compo et al., 2011). The current version 20CRv3 (Slivinski et al., 2019) starts in

102   1806 and comprises 80 members, with a spatial resolution is ca. 0.7° x 0.7°. It assimilates data from

103   the International Surface Pressure Databank (ISPD) Version 4.7 (Cram et al., 2015). We use 20CRv3

104   for our study and aim to assimilate additional observations. As we perform the assimilation off-line

105   (i.e., we do not cycle the analysis field back to the next model forecast step), the state vector does not

106   need to cover the full model state. For our analysis we use the fields of the Southern Hemisphere for

107   temperature and SLP at 12 UTC, from 1901 to 1930.

108   **2.3   Processing of observations**

109   All observations were first debiased relative to 20CRv3. For station temperature data we fitted the

110   first two harmonics of the seasonal cycle to both observations and 20CRv3 and subtracted the

111   difference. For pressure data (including the ship data), we corrected only the mean bias. We used the

112   overlap between observations and 20CRv3 in period 1901-1930 for debiasing (although the ship

113   records are much shorter).

114   For the assimilation of temperature, we assume an error of 3^2 K^2, similar as in Brönnimann (2022), for

115   SLP 3^2 hPa^2. Note that this concerns the difference between the data from the closest grid point

116   extracted from 20CRv3 and the observations. Thus, it accounts for the errors in the measurement

117   itself, the processing (Brugnara et al., 2015), and the representativity of the grid point but not the error

118   in 20CRv3 itself. Note that the debiasing step removes part of the systematic error.

119   **2.4   Offline data assimilation method**

120   The assimilation uses the Ensemble Square Root filter (Whitaker and Hamill, 2002) to assimilate

121   historical observations **y** into the 80 member ensemble of 20CRv3 (**x$_b$**), yielding **x$_a$**. For the following

122   see Brönnimann (2022).

123   First the ensemble mean is updated and then anomalies from the mean:

124    $$\overline{\mathbf{x_a}} = \overline{\mathbf{x_b}} + \mathbf{K}\left(\overline{\mathbf{y}} - \mathbf{H}\overline{\mathbf{x_b}}\right) \tag{1}$$

125    $$\mathbf{x'_a} = \mathbf{x'_b} + \widetilde{\mathbf{K}}(\mathbf{y'} - \mathbf{H}\mathbf{x'_b}) = \left(\mathbf{I} - \widetilde{\mathbf{K}}\mathbf{H}\right)\mathbf{x'_b}, \text{with}: \mathbf{y'} = 0 \tag{2}$$

126   **H** is the Jacobian matrix of the linear observation operator that extracts the observation from the model

127   state. The Kalman gain matrix **K** for the ensemble mean and the anomalies from the mean is defined

128   as:

129    $$\mathbf{K} = \mathbf{P^b}\mathbf{H^T}\left(\mathbf{H}\mathbf{P^b}\mathbf{H^T} + \mathbf{R}\right)^{-1} \tag{3}$$

130    $$\widetilde{\mathbf{K}} = \mathbf{P^b}\mathbf{H^T}\left[\left(\sqrt{\mathbf{H}\mathbf{P^b}\mathbf{H^T} + \mathbf{R}}\right)^{-1}\right]^{\mathbf{T}} \times \left(\sqrt{\mathbf{H}\mathbf{P^b}\mathbf{H^T} + \mathbf{R}} + \sqrt{\mathbf{R}}\right)^{-1} \tag{4}$$

131   **P^b** and **R** are the background error and observation error covariance matrices, respectively. The

132   former is calculated from the 80 members; no localisation was performed. The latter is assumed

133   diagonal. We did not store all 80 updated members, but only the ensemble mean and the ensemble

134   spread. The data set is published along with this paper in a repository (Brönnimann, 2023). The

135   assimilation was performed for the period 1901-1930. Outliers were removed **y–Hx** was larger than 3

136     $\times$ (**$HP^bH^T + R$**)$^{0.5}$.

137   The results were evaluated by means of the Pearson correlation and root mean squared error (RMSE)

138   at the observation locations (again, the mean annual temperature cycle was removed beforehand by

139   fitting the first two harmonics) as well as the reduction of the ensemble standard deviation. Note that a

140   full leave-one-out approach would be computationally expensive and of little value as measurements

141   are typically far apart from each other (results are expected to be similar as described in Brönnimann

142   (2022) for 1877/78, i.e., rather small but consistent improvements). We show results from a leave-

143   one-out approach only for a case when several observations were close together. As the assimilation is

144   offline and only few observations are available, the fields for each individual day only show

145   improvement in a few spotlight locations. Therefore, in the following, we aggregate the daily fields to

146   seasonal, annual or zonal means. At the same time, as all observations are debiased relative to

147   20CRv3, they will not have an effect on the long-term average.

148

2.5   Other data sets

150   For further analyses we used the temperature data sets HadCRUT5 (Morice et al., 2021), GISTEMP

151   (Lensson et al., 2019; GISTEMP Team, 2023) , NOAAGlobalTemp (Huang et al., 2020), and

152   Berkeley Earth BEST (Rohde and Housefather, 2020). We also analysed the original 20CRv3 output

153   as well as the monthly global climate reconstruction ModE-RA (Modern Era Reanalysis), which is

154   based on assimilating historical observations (including ship-based pressure observations) and proxies

155   into a 20 member ensemble of atmospheric model simulation (termed ModE-Sim) in a similar way as

156   in this paper (Valler et al., 2023ab). The data set is focusing on the period prior to 1890, and therefore

157   the input data is "frozen" at that year.

158   The model simulations ModE-Sim, which we also analysed, were driven by SSTs from HadISST

159   (Titchner and Rayner, 2014) volcanic and solar forcing (for details see Hand et al., 2023). Note that

160   these data sets (20CRv3, HadCRUT5, ModE-RA, ModE-Sim) use very similar SST data. Hence they

161   are not independent of each other. We therefore also analysed ModE-RAclim, which is the same as

162   ModE-RA except that it uses a random selection of 100 model years and ensemble members from

163   ModE-Sim as prior. Hence, this data set does not see the SST forcing. Note that ModE-RAclim and

164   ModE-Sim are mutually independent. For all these data sets we used the ensemble mean.

165   Finally, we also used the seasonal SLP reconstructions for Antarctica from Fogt and Connolly (2021),

166   which reach back to 1905. As recommended by the authors, we used the standard reconstruction for

167   Dec.-Feb. and the pseudo reconstruction for all other seasons. Note that these data were not

168   assimilated into ModE-RA.

Climate
of the Past
Discussions

169 **2.6   Analysis**

170 A preliminary analysis of Southern Hemisphere temperature from HadCRUT5 (Fig. 3, annual means)

171 shows that the coldest multiyear period in the record was from 1908-1911 (grey shaded). We

172 therefore focus on this four-year period in the following and analyse this period relative to the 1901-

173 1930 mean, which is also the period over which the assimilation was performed.
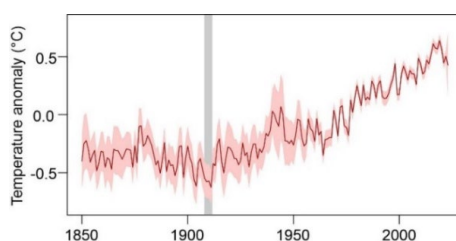
174

175 **Fig. 3.** Southern Hemisphere mean annual mean temperatures relative to the 1961-1990 reference period from

176 HadCRUT5 with 2.5% to 97.5% uncertainty range (grey).

177

178 This period is analysed first on the level of annual means in all available data sets. The standard

179 deviation of interannual variability is used to measure the magnitude of the anomalies. We then turn

180 to the seasonal scale and focus on atmospheric circulation as expressed in SLP.

181 **3   Results**

182 **3.1   Evaluation**

183 An analysis of correlations between 20CRv3 and the additionally digitised ship data shows that the

184 latter fit well with 20CRv3 (Table 1). One ship with a short record and many outliers exhibits a

185 correlation of only 0.71, the other ships show correlations between the 0.76 to 0.94. This points to the

186 already excellent quality of 20CRv3. Almost by construction, the assimilation approach greatly

187 improves the correlation to values of typically around 0.95 (the above-mentioned ship is an exception

188 to this).

189 The assimilation of additional data reduces the ensemble spread (Fig. 4, top). The spread reduction is

190 larger near land stations, where measurements are always available. A reduction is also seen in SLP

191 near the ship tracks, but since there were only few ships in the vast space, the reduction is statistically

192 weak, typically between 0.9 to 0.95 along the ship tracks.

193 The effect of the assimilation is illustrated for the example of 17 February 1909 in the lower part of

194 Fig. 4. On this day, five observations (two ship-based pressure measurements and three land-based

195 temperature measurements) were close to each other. For this case we performed a leave-one-out

196 approach. The raw 20CRv3 data show a high pressure system centred over Tasmania, which is further

197 strengthened and southward extended in 20CRv3+. In fact, the lower figure shows that both ships

198 indicated higher SLP than 20CRv3 (leftmost half-circle). Not surprisingly, in the leave-one-out

199 approach the pressure is increased at both locations due to the mutual effects of the two ships. The

200 departure from observations further increases in the full assimilation. Interestingly, the largest change

201 due to the assimilation does not occur exactly at the assimilation location, but to the south. Also, the

202 assimilation leads to a pressure decrease over some subpolar regions.

203
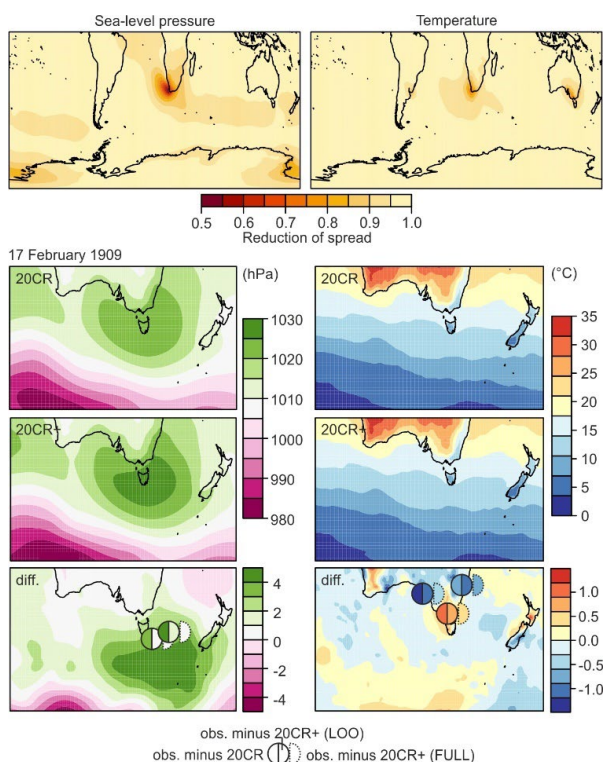
Fig. 4. Results of the evaluation of the assimilation approach. Top: Reduction of the average ensemble spread for SLP and
temperature. Bottom: Results from the leave-one-out (LOO) approach for 17 February 1909 over Southern Australia.

207 For temperature, the situation is more complex as observations from Kent Town (Adelaide) and

208 Sydney were cooler than 20CR, whereas measurements from Melbourne were warmer. In Kent Town

209 and Melbourne, the leave-one-out approach reduces this departure. Hence, the stations mutually

210 correct each other in the right direction. An exception is Sydney, where the departure becomes

211 slightly larger when assimilating only all neighbouring stations. As for pressure, we note that the

212 change due to the assimilation is non-local and appears rather noisy with effects relatively far away

213 from observations. This is due to the imperfect estimation of the covariance matrix based on the 80

214 members. Localisation would help to remove this effect. On the other hand, the changes are typically

215 not very large.

3.2   Temperature

After having evaluated the assimilation, we turn to the analysis of the temperature. Annual mean
temperature anomaly maps are shown in Fig. 5 (top) for four available observation-based temperature
products. All show a general cooling, with particular cool spots in the southern tropical and
subtropical Atlantic, the tropical Pacific, and the South Pacific. Some land areas of the southern
midlatitudes were cold, too. Conversely, the ocean was warm around the Antarctic Peninsula.
However, the data basis is sparse and hence differences between different products considerable. The
middle and bottom part of the figure show results from assimilation approaches that incorporate
pressure and other variables. 20CRv3 shows a rather similar pattern as the observation-based data
sets. Over the ocean this is due to the fact that the model uses observed SSTs as boundary conditions,
but there is also agreement over land. For instance, as the observation-based products, 20CRv3
indicates low temperatures over Australia. The assimilation of additional data has only a very small
effect that is hardly visible when plotting only the anomaly field. Only when directly plotting the
difference one sees that the additionally assimilated information produces slightly warmer conditions
over Southern Australia.
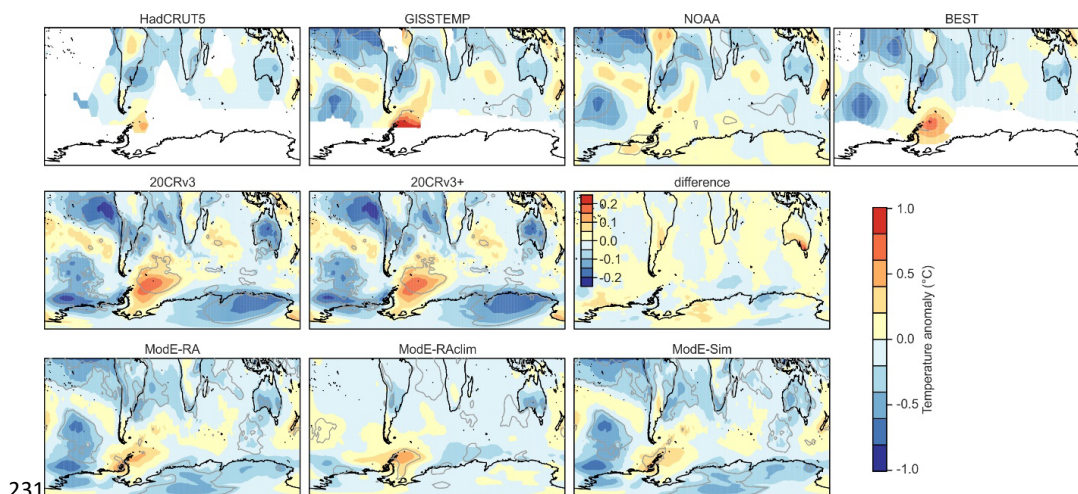
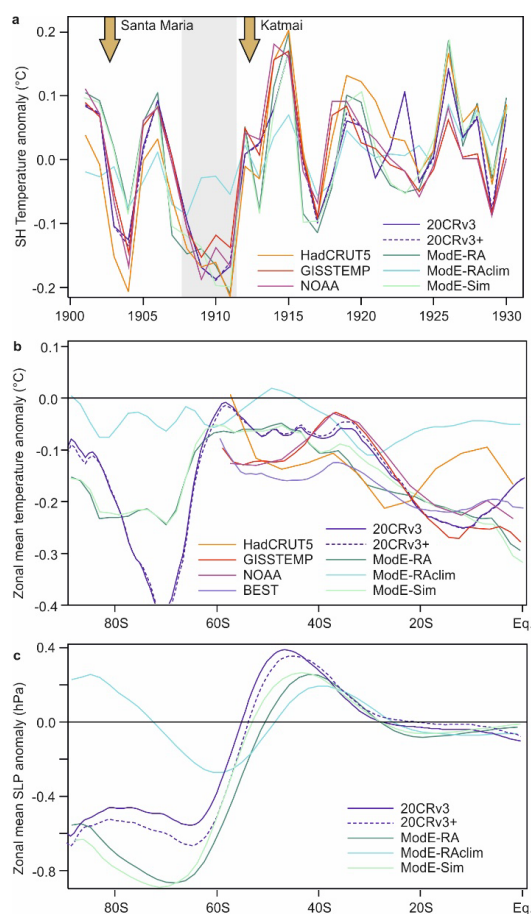**Fig. 5.** Annual mean temperature difference between 1908-1911 and the remaining years in the 1901-1930
period in (top row) four observational data sets, middle row: 20CRv3 and 20CRv3+ as well as their difference,
and (bottom row) ModE-RA, ModE-RAclim, and ModE-Sim. Grey lines indicate where the 4-year anomaly
exceeds one standard deviation of the interannual variability of the annual mean in 1901-1930. The number of
missing values was not restricted.

While 20CRv3 only assimilated pressure data, ModE-RA (shown in the lower row) also assimilates
temperature; the resulting temperature anomaly map looks again very similar as that of all other
products. However, ModE-RA allows to disentangle where the information comes from. ModE-Sim
(lower right) indicates the pure atmospheric simulations, which again reproduce many of the

9

Climate
of the Past
Discussions

241   temperature features also over land. ModE-RAclim, in turn, only sees climatological SSTs and thus

242   shows the effect of only the observations. Interestingly, also ModE-RAclim shows a very similar

243   pattern. Note that ModE-RAclim and ModE-Sim are independent.

244   Time series of Southern Hemisphere temperature from these data sets (Fig. 6a) show a relatively good

245   agreement between the data sets over time. The period 1908-1911 stands out as the coldest 4-year

246   interval within the displayed period. The preceding drop as well as the small subsequent drop coincide

247   with volcanic eruptions. The good agreement between the data sets is partly due to similar SSTs used

248   in the different approaches. ModE-RAclim, which does not see SSTs or volcanic eruptions, shows a

249   weaker cooling for 1908-1911 (though still a cooling) but does show the cooling spikes before and

250   after.

251

252   **Fig. 6.** Southern Hemisphere annual mean average temperature (anomaly from 1901-1930) in different data sets

253   (**a**). Zonal mean annual mean difference between 1908-1911 and the 1901-1930 climatology for temperature (**b**)

254   and SLP (**c**) in different data sets.

3.3 Pressure

The SLP anomaly field (Fig. 7) is again similar in 20CRv3 and in ModE-RA. In 20CRv3, the assimilation has a slightly larger impact on SLP than on temperature. Specifically, the assimilation leads to lower SLP in the Amundsen-Bellingshausen Sea area but also over the Southern Indian Ocean. ModE-RA again shows a good agreement between the pure simulation (which is arguably strongly affected by SSTs), the effect of only the observations, and the combined effect. Altogether, the fields indicate a positive SAM, although it should be noted that hardly any pressure data from the southern high latitudes enters any of the products.
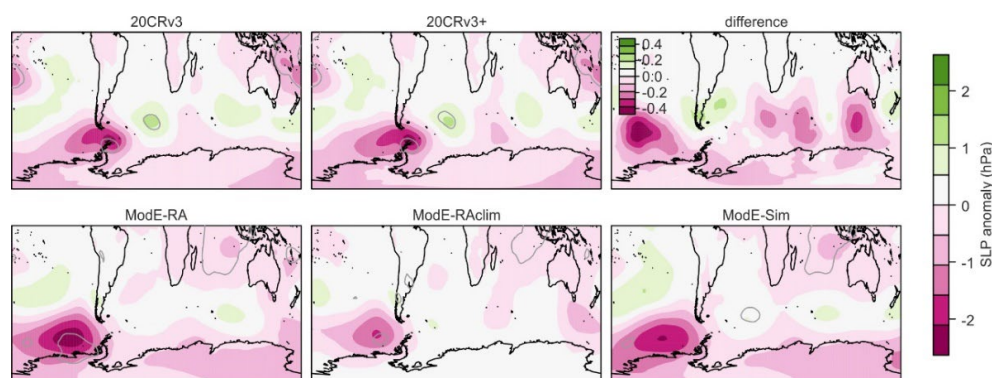
Fig. 7. Annual mean SLP difference between 1908-1911 and the remaining years in the 1901-1930 period in (top) 20CRv3 and 20CRv3+ as well as their difference, and (bottom) ModE-RA, ModE-RAclim, and ModE-Sim. Grey lines indicate where the 4-year anomaly exceeds one standard deviation of the interannual variability of the annual mean in 1901-1930.

In the next step we analysed zonally averaged temperature and SLP in 20CRv3 and 20CRv3+ (Fig. 6b,c) in order to obtain a better view of the possible SAM variability and of the changes induced by the assimilation to SLP and temperature. With respect to temperature, it becomes clear that the assimilation of additional observations (although most of them were pressure) led to a slightly smaller cooling at southern mid-to-high latitudes. However, the much larger signal is that in the tropics, which remains unaffected (note that only ships in the tropical Atlantic were assimilated).

The corresponding plot for SLP shows the sign of a positive SAM, with positive anomalies at mid latitudes and negative in the subpolar regions. This is slightly amplified in 20CRv3+. Interestingly, even ModE-RAclim, which does not see forcings, shows a very similar pattern as the other products north of 60° S. In the following we first focus on this change in the polar and subpolar circulation, then we address the circulation in the tropical region.

The strengthened SAM and specifically the strengthened Amundsen-Bellingshausen seas Low is further analysed on a seasonal scale by comparing 20CRv3+ and ModE-RA with the Fogt and Connolly (2021) data (Fig. 8). While all show a strengthening of the Amundsen-Bellingshausen seas

282 low, there are clear differences in the seasonal expression. ModE-RA has the strongest signal in fall,

283 20CRv3+ and Fogt and Connolly (2021) have the strongest signal in winter. Without further

284 information, it is impossible to rule out one or the other analysis, but it shows that there is still large

285 uncertainty with respect to Antarctic SLP despite the relatively good agreement on the annual mean

286 anomaly over this 4-year period.

287 Finally, we analysed the tropical atmospheric circulation. Figure 9 shows the SOI calculated in the

288 five data sets used in this study that contain SLP data. Generally, all data sets suggest a strengthened

289 Walker circulation around 1910, and the correlation between different data sets is relatively good.

290 Overall, however, the 1908-1911 period does not stand out as an extremely anomalous period in the

291 tropical Pacific.

292
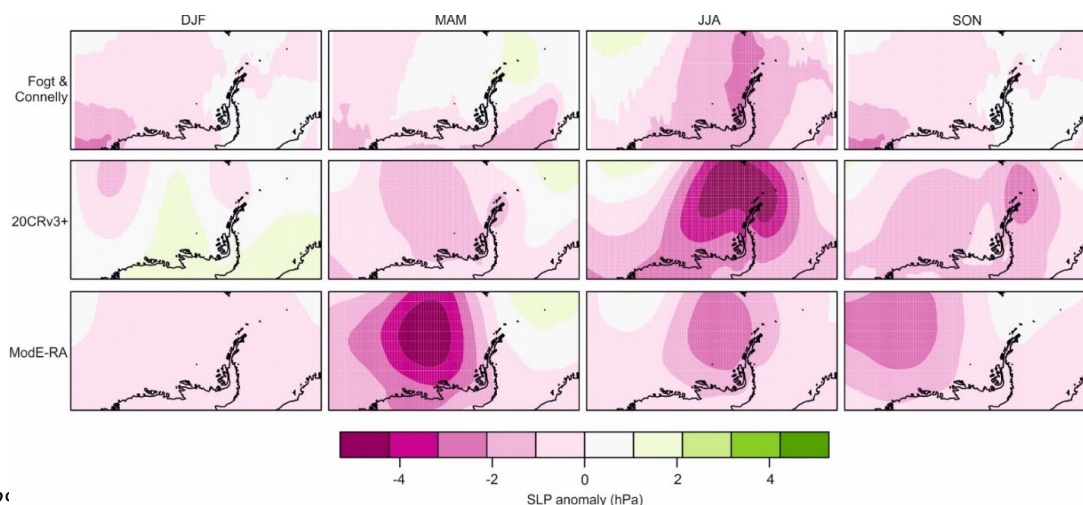
294 **Fig. 8.** Seasonal maps of SLP deviations in 1908-1911 from the 1901-1930 climatology for three different data
295 sets.
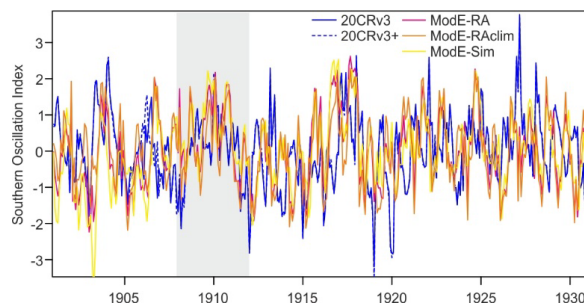
297 **Fig. 9.** Southern Oscillation Index calculated from 20CRv3, 20CRv3+, ModE-RA, ModE-RAclim, and ModE-
298 Sim calculated from the 1901-1930 climatology.

299 4   Discussion

300   The goal of this study was to generate improved data products to study the early 20th century cool
301   period by digitising additional data and assimilating them into 20CRv3. A reduction of the spread
302   could be achieved, and effects of the observations are clearly seen, although the overall effects on the
303   4-year averaged anomaly are small for temperature. At the same time, it should be noted that a large
304   amount of observations would still be available and await to be rescued, and our study has shown that
305   they could provide a large additional benefit.

306   The comparison of very different products such as 20CRv3, the different ModE-RA products, and the
307   Fogt and Connolly (2021) SLP proved beneficial and also indicated a robustness of the signal, despite
308   significant seasonal differences.

309   The analysis of different products for temperature and SLP for the years around 1910 in the Southern
310   Hemisphere showed a good agreement of the spatial pattern relative to neighbouring years, at least on
311   the annual mean scale. It should be noted, however, that a good agreement does not imply a small
312   uncertainty as some of the data sets are based on very similar input. For instance, all use HadISST1.1
313   or similar for SSTs, and both ModE-RA and 20CRv3 use SLP (HadCRUT5 and ModE-RA both use
314   land temperature data).

315   The assimilation of additional data into 20CRv3 leads to a slightly weaker cooling signal, but the
316   magnitude of the difference is small. This might partly be due to the debiasing, which removes any
317   signal at the scale of the length of the records. As most records (notably, the ship data) are short, their
318   contribution to a 4-yr signal is necessarily weak. In all, the assimilation shows that the amplitude of
319   the cooling is not well constrained with the additional data. Further data are needed to better
320   understand the cooling phase.

321   A cooling phase nevertheless remains, and this cooling phase in the Southern midlatitudes around
322   1910 is a relevant period for better understanding natural decadal climate variability. The SST
323   anomaly fields resembles a La Niña pattern (see also Fogt and Connolly, 2021), and the SOI indicates
324   a strengthened Walker circulation around 1910. The general pattern of cooling as well as the pattern
325   of SLP anomalies is very similar in all data sets, but overall the anomaly during these years does not
326   seem to be extremely strong.

327   All data sets consistently show a neutral to positive SAM, in 20CRv3+ the positive SAM is even
328   amplified. The SST pattern is generally consistent with a positive SAM (e.g., Hartmann, 2022, for a
329   wind-based SAM index in Oct-Mar). The relation between La Niña conditions and a strong
330   Amundsen sea low is also well known (Turner et al., 2013). Furthermore, the temperature anomaly
331   pattern also resembles other suggested modes of variability such as the Subtropical Indian Ocean
332   Dipole Mode or Southern Suptropical Atlantic Dipole Mode (e.g., Wainer et al., 2021; Yu et al.,
333   2023), whose behaviour in the early 20th century is however not well known.

334   Finally, it should be noted that the first part of the 20th century also saw two large volcanic eruptions,

335   namely Santa Maria in 1902 and Novarupta in 1912. The former was a tropical eruption that might

336   have affected the Southern Hemisphere and had a global cooling effect; many ship logs from the

337   Southern Ocean for these years have been imaged and await digitisation. The latter was a northern

338   high-latitude eruption and might not have affected the Southern Hemisphere strongly, but the effect

339   on Northern Hemisphere temperature is well studied (e.g., Oman et al., 2005). Two cooling spikes are

340   seen in the Southern Hemisphere temperature series following these two eruptions, indicating a

341   volcanic contribution to the cooling.

342   Taken together, the global cooling episode in the early 20th century, which peaks in 1908-1911, seems

343   to be a combination of two volcanic eruptions, a strengthened Walker circulation around 1910, a

344   positive SAM, and concurrent states in the South Atlantic and Indian Ocean Modes of variability.

345   Although data uncertainty remains high, different data sets are consistent with each other and the

346   patterns found are consistent with literature findings, thus supporting that the globally cool episode in

347   the early 20th century was real. The ETCW, which was mostly studied with respect to Northern

348   Hemispheric anomalies and the question of a warm phase in the 1940s (Brönnimann, 2009), emerged

349   from a cold climate state strongest in the Southern Hemisphere.

350   **5   Conclusions**

351   A global cold period from 1908 to 1911 was analysed based on reanalysis data and observations. The

352   cooling was most pronounced over the Southern Ocean, where available observations are few and far

353   apart. Therefore, we digitized additional data from ship from the Southern Hemisphere from 1902-

354   1916. These data, together with six land station records, were then assimilated offline into the 80-

355   member ensemble of 20CRv3. The new data confirmed the temperature and pressure anomaly

356   patterns found in 20CRv3. However, they decrease the ensemble spread, thus contributing to a smaller

357   uncertainty of the analysis of atmospheric circulation. Overall, we find a positive SAM, which is even

358   amplified in 20CRv3+. This is due to a strengthened Amundsen-Bellingshausen seas low, which is

359   identified in all data sets. Differences between data sets emerge when analysing the seasonal timing of

360   the anomalies.

361   SST and SLP patterns indicate a La Niña tendency and a strengthened Walker circulation around

362   1910, which is consistent with the strengthened Amundsen-Bellingshausen seas low. SST patterns in

363   the South Atlantic and South Indian Ocean also are consistent with modes discussed in the literature.

364   All of this results point to a real climatic phenomenon as the cause of the 1908-1911 cold anomaly

365   and not a data artefact. Atmospheric model simulations using SSTs and external forcings as boundary

366   conditions reproduce the main features of the SLP anomaly fields over the Southern Hemisphere

367   found in a data set based only on observations. This again indicates that the temperature anomaly is

368   physically consistent with all other information and perhaps an ocean-forced signal. Most importantly,

Climate
of the Past
Discussions

369   the period was preceded and followed by two volcanic eruptions, leading to global cooling. The

370   eruptions and the cold 1908-1911 period together provided a cold start into the ETCW.

371   Finally, the newly digitised ship log book data constitute only a small fraction of the non-digitised

372   (but imaged) log book data. Digitising the vast amount of marine data from the early 20th century

373   could help to generate an improved version of 20CR that would provide further insights into this cold

374   period.

380   **Contributions:** YB coordinated the digitisation, processed, quality-controlled, and formatted the data. SB

381   performed the assimilation and the analyses, CW imaged and provided the log books. All authors commented on

382   the manuscript.

383   **Competing interests:** The authors declare no competing financial interests.

384   **Data availability statement:** The 20CRv3+ data set, including the station and ship input data and the R code

385   for the pre-processing and assimilation is available from Brönnimann (2023). The digitised ship log data have

386   been sent to ICOADS (Freeman et al., 2017). The 20CRv3 data (Slivinski et al., 2019) can be downloaded from

387   NCAR (https://rda.ucar.edu/datasets/ds131.3/, DOI: 10.5065/H93G-WS83, downloaded 7 Oct. 2022, last

388   accessed 11 Oct 2023). The ModE-RA data (Valler et al., 2023a) can be downloaded from DKRZ

389   (https://www.wdc-climate.de/ui/entry?acronym=ModE-RA). Antarctic SLP fields are available from Fogt and

390   Connolly (2021), HadCRUT5 is downloadable from https://www.metoffice.gov.uk/hadobs/hadcrut5/

391   (downloaded 14 Jul. 2023, last accessed 11 Oct. 2023). GISTEMP was obtained from the NASA Goddard

392   Institute for Space Studies (GISTEMP Team, 2023, downloaded 18 Jul. 2023, last accessed 11 Oct. 2023 at

393   https://data.giss.nasa.gov/gistemp/). The BEST data Rohde and Hausfather, 2020) were obtained from

394   https://berkeleyearth.org/data/ (downloaded 17 Jul. 2023, last accessed 11 Oct. 2023). NOAAGlobalTemp

395   version 5 (Huang et al., 2020) was downloaded from https://www.ncei.noaa.gov/products/land-based-

396   station/noaa-global-temp (downloaded 17 Jul. 2023, last accessed 11 Oc.t 2023).

References

398   Abram, N., Mulvaney, R., Vimeux, F., Phipps, S. J., Turner, J. and England, M. H.: Evolution of the Southern

399   Annular Mode during the past millennium, Nature Clim Change, 4, 564–569,

400   https://doi.org/10.1038/nclimate2235, 2014.

401   Brönnimann, S.: Early twentieth-century warming, Nature Geosci., 2, 735-736, 2009.

402   Brönnimann, S.: Historical Observations for Improving Reanalyses, Front. Clim. 4, 880473, 2022.

403   Brönnimann, S.: Daily temperature and sea-level pressure fields for the Southern Hemisphere 1901-1930.

404   BORIS Portal, https://doi.org/10.48620/371, 2023.

405 Brugnara, Y., Auchmann, R., Brönnimann, S., Allan, R. J., Auer, I., Barriendos, M., Bergström, H., Bhend, J.,
406   Brázdil, R., Compo, G. P., Cornes, R. C., Dominguez-Castro, F., van Engelen, A. F. V., Filipiak, J.,
407   Holopainen, J., Jourdain, S., Kunz, M., Luterbacher, J., Maugeri, M., Mercalli, L., Moberg, A., Mock, C. J.,
408   Pichard, G., Řezníčková, L., van der Schrier, G., Slonosky, V., Ustrnul, Z., Valente, M. A., Wypych, A., and
409   Yin, X.: A collection of sub-daily pressure and temperature observations for the early instrumental period
410   with a focus on the "year without a summer" 1816, Clim. Past, 11, 1027–1047, https://doi.org/10.5194/cp-
411   11-1027-2015, 2015.

412 Cane, M. A.: The evolution of El Niño, past and future, Earth Planet. Sci. Lett., 230, 227-240, 2005.

413 Compo, G. P., Whitaker, J. S., Sardeshmukh, P. D., Matsui, N., Allan, R. J., Yin, X., Gleason, B. E., Vose, R.
414   S., Rutledge, G., Bessemoulin, P., Brönnimann, S., Brunet, M., Crouthamel, R. I., Grant, A. N., Groisman,
415   P. Y., Jones, P. D., Kruk, M. C., Kruger, A. C., Marshall, G. J., Maugeri, M., Mok, H. Y., Nordli, Ø., Ross,
416   T. F., Trigo, R. M., Wang, X. L., Woodruff, S. D., and Worley, S. J.: The Twentieth Century Reanalysis
417   Project, Q. J. Roy. Meteor. Soc., 137, 1–28, 2011.

418 Connolly, C.: Causes of Southern Hemisphere climate variability in the early 20th century, Thesis, Ohio
419   University, 2020.

420 Cram, T. A., Compo, G. P., Yin, X., Allan, R. J., McColl, C., Vose, R. S., Whitaker, J. S., Matsui, N., Ashcroft,
421   L., Auchmann, R., Bessemoulin, P., Brandsma, T., Brohan, P., Brunet, M., Comeaux, J., Crouthamel, R.,
422   Gleason Jr., B. E., Groisman, P. Y., Hersbach, H., Jones, P. D., Jónsson, T., Jourdain, S., Kelly, G., Knapp,
423   K. R., Kruger, A., Kubota, H., Lentini, G., Lorrey, A., Lott, N., Lubker, S. J., Luterbacher, J., Marshall, G.
424   J., Maugeri, M., Mock, C. J., Mok, H. Y., Nordli, Ø., Rodwell, M., Ross, T. F., Schuster, D., Srnec, L.,
425   Valente, M. A., Vizi, Z., Wang, X. L., Westcott, N., Woollen, J. S., and Worley, S. J.: The International
426   Surface Pressure Databank version 2, Geosci. Data J., 2, 31–46, 2015.

427 Fogt, R. L. and Connolly, C. J.: Extratropical Southern Hemisphere Synchronous Pressure Variability in the
428   Early Twentieth Century, J. Clim., 34, 5795–5811, https://doi.org/10.1175/JCLI-D-20-0498.1, 2021.

429 Freeman, E., Woodruff, S. D., Worley, S. J., Lubker, S. J., Kent, E. C., Angel, W. E., Berry, D. I., Brohan, P.,
430   Eastman, R., Gates, L., Gloeden, W., Ji, Z., Lawrimore, J., Rayner, N. A., Rosenhagen, G., and Smith, S. R.:
431   ICOADS Release 3.0: a major update to the historical marine climate record, Int. J. Climatol., 37, 2211-
432   2232, https://doi.org/10.1002/joc.4775, 2017.

433 GISTEMP Team: GISS Surface Temperature Analysis (GISTEMP), version 4. NASA Goddard Institute for
434   Space Studies, 2023, dataset accessed 2023-07-18 at https://data.giss.nasa.gov/gistemp/.

435 Hand, R., Samakinwa, E., Lipfert, L., and Brönnimann S.: ModE-Sim – A medium size AGCM ensemble to
436   study climate variability during the past 600 years, Geosci. Model Dev., 16, 4853–4866, 2023.

437 Hartmann, D. L.: The Antarctic ozone hole and the pattern effect on climate sensitivity, Proc. Natl. Acad. Sci.
438   119, e22078891, 2022.

439 Hegerl, G. C., Brönnimann, S., Schurer, A. and Cowan T.: The early 20th century warming: Anomalies, causes,
440   and consequences, WIREs Clim Change 9, e522, https://doi.org/10.1002/wcc.522, 2018.

441 Huang, B., Menne, M. J., Boyer, T., Freeman, E., Gleason, B. E., Lawrimore, J. H., Liu, C., Rennie, J. J.,
442   Schreck, C., Sun, F., Vose, R., Williams, C. N., Yin, X., and Zhang, H.-M.: Uncertainty estimates for sea

443   surface temperature and land surface air temperature in NOAAGlobalTemp version 5, J. Clim., 33, 1351-
444   1379, https://doi.org/10.1175/JCLI-D-19-0395.1, 2020.

445   Lenssen, N., Schmidt, G., Hansen, J., Menne, M., Persin, A,. Ruedy, R., and Zyss, D.: Improvements in the
446   GISTEMP uncertainty model, J. Geophys. Res., 124, 6307-6326, https://doi.org/10.1029/2018JD029522,
447   2019.

448   Morice, C. P., Kennedy, J. J, Rayner, N. A., Winn, J. P., Hogan, E., Killick, R. E., Dunn, R. J. H., Osborn, T. J.,
449   Jones, P. D., and Simpson, I. R.: An updated assessment of near-surface temperature change from 1850: the
450   HadCRUT5 data set. J. Geophys. Res. 126, e2019JD032361, https://doi.org/10.1029/2019JD032361, 2021

451   Oman, L., Robock, A., Stenchikov, G., Schmidt, G. A., and Ruedy, R.: Climatic response to high-latitude
452   volcanic eruptions, J. Geophys. Res., 110, D13103, https://doi.org/10.1029/2004JD005487, 2005.

453   Rohde, R. A. and Hausfather, Z.: The Berkeley Earth Land/Ocean Temperature Record, Earth Syst. Sci. Data,
454   12, 3469-3479, 2020, https://doi.org/10.5194/essd-12-3469-2020.

455   Slivinski, L. C., Compo, G. P., Whitaker, J. S., Sardeshmukh, P. D., Giese, B. S., McColl, C., Allan, R., Yin, X.,
456   Vose, R., Titchner, H., Kennedy, J., Spencer, L. J., Ashcroft, L., Brönnimann, S., Brunet, M., Camuffo, D.,
457   Cornes, R., Cram, T. A., Crouthamel, R., Domínguez-Castro, F., Freeman, J. E., Gergis, J., Hawkins, E.,
458   Jones, P. D., Jourdain, S., Kaplan, A., Kubota, H., Le Blancq, F., Lee, T., Lorrey, A., Luterbacher, J.,
459   Maugeri, M., Mock, C. J., Moore, G. K., Przybylak, R., Pudmenzky, C., Reason, C., Slonosky, V. C., Smith,
460   C., Tinz, B., Trewin, B., Valente, M. A., Wang, X. L., Wilkinson, C., Wood, K., and Wyszyński, P.:
461   Towards a more reliable historical reanalysis: Improvements to the Twentieth Century Reanalysis system, Q.
462   J. Roy. Meteorol. Soc., 145, 2876–2908, https://doi.org/10.1002/qj.3598, 2019.

463   Titchner, H. A., and Rayner, N. A.: The Met Office Hadley Centre sea ice and sea surface temperature data set,
464   version 2: 1. Sea ice concentrations, J. Geophys. Res., 119, 2864-2889,
465   https://doi.org/10.1002/2013JD020316, 2014.

466   Turner, J., Phillips, T., Hosking, J.S., Marshall, G.J. and Orr, A.: The Amundsen Sea low, Int. J. Climatol., 33,
467   1818-1829, https://doi.org/10.1002/joc.3558, 2013.

468   Valler, V., Franke, J. Brugnara, Y. Samakinwa, E. Hand, R. Burgdorf, A.-M. Lipfert, L. Friedman, A. Lundstad,
469   E. and Brönnimann, S.: ModE-RA - A global monthly paleo-reanalysis to study climate variability during
470   the past 600 years, World Data Center for Climate (WDCC) at DKRZ, https://www.wdc-
471   climate.de/ui/entry?acronym=ModE-RA, 2023a.

472   Valler, V., Franke, J. Brugnara, Y. Samakinwa, E. Hand, R. Burgdorf, A.-M. Lipfert, L. Friedman, A. Lundstad,
473   E. and Brönnimann, S.: ModE-RA - a global monthly paleo-reanalysis of the modern era (1421-2008), Sci.
474   Data (accepted), 2023b.

475   Wainer, I., Prado, L.F., Khodri, M., and Otto-Bliesenr, B.: The South Atlantic sub-tropical dipole mode since
476   the last deglaciation and changes in rainfall, Clim. Dyn., 56, 109–122, https://doi.org/10.1007/s00382-020-
477   05468-z, 2021.

478   Whitaker, J., and Hamill, T. M.: Ensemble data assimilation without perturbed observations, Mon. Wea. Rev.,
479   130, 1913–1924, 2002.

480   Yu, L., Zhong, S., Vihma, T., Sui, C., and Sun, B.: A change in the relation between the Subtropical Indian
481   Ocean Dipole and the South Atlantic Ocean Dipole indices in the past four decades, Atmos. Chem. Phys.,
482   23, 345–353, https://doi.org/10.5194/acp-23-345-2023, 2023.